

OASIS Survey Direct Imaging and Astrometric Discovery of HIP 71618 B: A Substellar Companion Suitable for the Roman Coronagraph Technology Demonstration*

MONA EL MORSY,¹ THAYNE CURRIE,^{1,2} BRIANNA LACY,³ TAYLOR L. TOBIN,⁴ QIER AN,⁵ YITING LI,⁴ ZIYING GU,⁶ MASAYUKI KUZUHARA,^{7,8} DANIELLE BOVIE,¹ DILLON PENG,⁹ JEFFREY CHILCOTE,⁹ OLIVIER GUYON,^{2,10} MILES LUCAS,^{11,2} TIMOTHY D BRANDT,¹² ROBERT DE ROSA,¹³ TYLER D GROFF,¹⁴ MARKUS JANSON,¹⁵ N. J. KASDIN,¹⁶ JULIEN LOZI,^{2,10} CHRISTIAN MAROIS,¹⁷ BERTRAND MENNESSON,¹⁸ NAOSHI MURAKAMI,^{7,8,19,20} ERIC NIELSEN,²¹ SABINA SAGYNBAYEVA,²² NOUR SKAF,²³ WILLIAM THOMPSON,¹⁷ MOTOHIDE TAMURA,^{10,8,6} TAICHI UYAMA,²⁴ ALICE ZURLO,^{25,26} VINCENT DEO,² AND SEBASTIEN VIEVARD²

¹Department of Physics and Astronomy, University of Texas at San Antonio, San Antonio, TX 78249, USA

²Subaru Telescope, National Astronomical Observatory of Japan, 650 North A'ohökü Place, Hilo, HI 96720, USA

³Department of Astronomy and Astrophysics, University of California-Santa Cruz, Santa Cruz, CA USA

⁴Department of Astronomy, University of Michigan, 1085 S. University, Ann Arbor, MI 48109, USA

⁵Department of Physics and Astronomy Johns Hopkins University, Baltimore, MD 21218, USA

⁶Department of Astronomy, Faculty of Science, The University of Tokyo, 7-3-1 Hongo, Bunkyo-ku, Tokyo 113-0033, Japan

⁷Astrobiology Center, NINS, 2-21-1 Osawa, Mitaka, Tokyo 181-8588, Japan

⁸National Astronomical Observatory of Japan, 2-21-1 Osawa, Mitaka, Tokyo 181-8588, Japan

⁹Department of Physics and Astronomy, University of Notre Dame, Nieuwland Science Hall, Notre Dame, IN 46556, USA

¹⁰Astrobiology Center, 2-21-1 Osawa, Mitaka, Tokyo 181-8588, Japan

¹¹Steward Observatory, University of Arizona, Tucson, AZ 85721, USA

¹²Space Telescope Science Institute, Baltimore, MD, USA

¹³European Southern Observatory, Alonso de Córdova 3107, Vitacura, Santiago, Chile

¹⁴NASA-Goddard Space Flight Center, Greenbelt, MD USA

¹⁵Department of Astronomy, Stockholm University, AlbaNova University Center, Stockholm, 10691, Sweden

¹⁶Department of Mechanical and Aerospace Engineering Princeton University, Princeton, New Jersey 08544, USA

¹⁷National Research Council, Herzberg Astronomy and Astrophysics, Victoria, BC, Canada

¹⁸Jet Propulsion Laboratory, California Institute of Technology, Pasadena, California, United States

¹⁹The Graduate University for Advanced Studies, SOKENDAI, 2-21-1 Osawa, Mitaka, Tokyo 181-8588, Japan

²⁰Faculty of Engineering, Hokkaido University, Kita 13, Nishi 8, Kita-ku, Sapporo, Hokkaido 060-8628, Japan

²¹Department of Astronomy, New Mexico State University, P. O. Box 30001, MSC 4500, Las Cruces, NM 88003, USA

²²Department of Physics and Astronomy, Stony Brook University, Stony Brook, NY 11794, USA

²³Institute for Astronomy, University of Hawai'i at Manoa, Hilo, HI 96720-2700, US

²⁴Department of Physics and Astronomy, California State University Northridge, 18111 Nordhoff Street, Northridge, CA 91330, USA

²⁵Instituto de Estudios Astrofísicos, Facultad de Ingeniería y Ciencias, Universidad Diego Portales, Av. Ejército Libertador 441, Santiago, Chile

²⁶Millennium Nucleus on Young Exoplanets and their Moons (YEMS)

ABSTRACT

We present the OASIS survey program discovery of a substellar companion orbiting the young A1V star HIP 71618, detected using precision astrometry from *Gaia* and *Hipparcos* and high-contrast imaging with SCEXAO/CHARIS and Keck/NIRC2. Atmospheric modeling favors a spectral type of M5–M8 and a temperature of $\sim 2700 \pm 100$ K. Dynamical modeling constrains HIP 71618 B's mass to be $60_{-21}^{+27} M_{\text{Jup}}$ or $65_{-29}^{+54} M_{\text{Jup}}$, depending on the adopted companion mass prior. It has a nearly-edge-on, 11 au orbit with a high eccentricity. HIP 71618 B will be located within Roman Coronagraph's dark hole region during the instrument's technological demonstration phase. A high signal-to-noise-ratio detection of HIP 71618 B at 575 nm would demonstrate a $5\text{-}\sigma$ contrast of 10^{-7} or better. The system is also located within or very close to Roman's Continuous Viewing Zone – near multiple candidate reference stars for dark-hole digging – and its primary is bright ($V \approx 5$). The suitability

of HIP 71618 as one potential Roman Coronagraph target for demonstrating the instrument’s core requirement (TTR5) should motivate the timely, deep vetting of candidate reference stars.

1. INTRODUCTION

High-contrast imaging observations over the past ~ 15 -20 years have revealed about two-dozen directly imaged superjovian planets (C. Marois et al. 2008; A. M. Lagrange et al. 2010; T. Currie et al. 2023a). Many recent planet imaging campaigns target stars based on direct, dynamical evidence for an imageable companion from Hipparcos and Gaia precision astrometry (e.g. T. Currie et al. 2023b; K. Franson et al. 2023; R. J. De Rosa et al. 2023; D. Mesa et al. 2023; M. El Morsy et al. 2024).

While still in their infancy, these surveys have already yielded the discovery of numerous substellar companions from ground-based adaptive optics (AO) assisted near-infrared (IR) data, including three superjovian planets (HIP 99770 b, AF Lep b, and HIP 54515 b) (T. Currie et al. 2020a; M. Kuzuhara et al. 2022; T. Currie et al. 2023b; R. J. De Rosa et al. 2023; D. Mesa et al. 2023; K. Franson et al. 2023; T. Currie et al. 2025). Compared to traditional, so-called “blind” or unbiased surveys (e.g. E. L. Nielsen et al. 2019), these campaigns appear to yield a higher rate of discoveries (M. El Morsy et al. 2024). Jointly modeling direct imaging and astrometric data can directly constrain the companions’ masses and improve orbital parameters estimates compared to direct imaging data alone (e.g. T. D. Brandt et al. 2019; G. M. Brandt et al. 2021).

The companions found from these direct imaging and astrometry programs are well-suited for detailed follow-up characterization and strategically important observations for NASA missions. Near-IR spectroscopic follow-up data better constrain companion chemistries and gravities (e.g. D. Bovie et al. 2025; M. El Morsy et al. 2025), including at moderate to high resolutions capable of constraining molecular abundances (W. O. Balmer et al. 2023, 2025; Y. Zhang et al. 2024; T. O. Winterhalder et al. 2025). Thermal IR follow-up (e.g. with JWST/NIRCam) can clarify atmospheric chemistry (K. Franson et al. 2024). Self-luminous substellar companions may have optical contrasts making them suitable for the critical Roman Coronagraph Instrument technology demonstration (B. Lacy & A. Burrows 2020).

In this Letter, we report the discovery of a brown dwarf orbiting ~ 11 au from the A-type star HIP 71618 from the Observing Accelerators with SCEXAO Imaging Survey (OASIS; PI: T. Currie, Co-PI: M. Kuzuhara M. El Morsy et al. 2024). The discovery combines precision astrometry from the Hipparcos-Gaia Catalogue of Accelerations (T. D. Brandt 2021), near-IR high-contrast direct imaging and spectroscopy from SCEXAO/CHARIS,

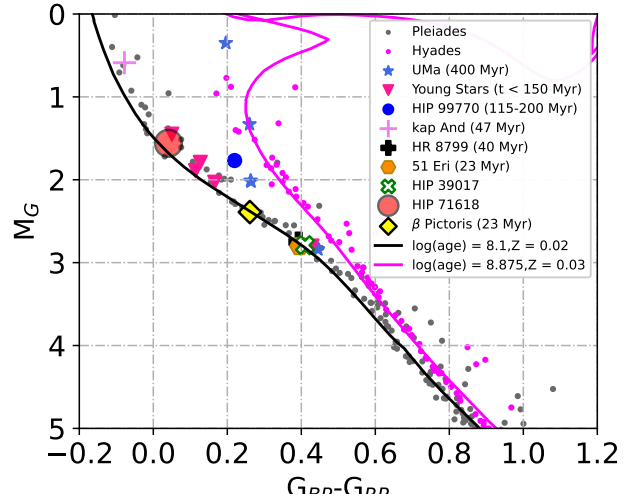


Figure 1. The *Gaia* color-magnitude diagram for the Pleiades (grey) and Hyades (dark red) compared to PARSEC isochrones for 112 Myr and 750 Myr, young stars with interferometrically measured ages $\lesssim 150$ Myr, stars in the 400 Myr-old Ursa Majoris Moving group, and other young stars with imaged substellar companions (J. Jones et al. 2015, 2016; J. W. Jones 2016; T. Currie et al. 2023b; T. L. Tobin et al. 2024).

and thermal IR imaging from Keck/NIRC2. In addition to being the second OASIS discovery, HIP 71618 B is the first substellar companion demonstrably suitable for the Roman Coronagraph Instrument’s Technology Demonstration.

2. PROPERTIES OF THE HIP 71618 SYSTEM

HIP 71618 (33 Boo, HD 129002) is a bright, nearby ($G = 5.38$, $d = 51.92$ pc) A1V (Gaia Collaboration et al. 2023). Banyan- Σ (J. Gagné et al. 2018) does not identify HIP 71618 as a high-confidence member of any known moving group ($p(\text{field}) \sim 98\%$, $p(\text{AB Dor}) \sim 2\%$) (J. Gagné et al. 2018). However, prior analyses based on color-magnitude diagrams find that the star is young, albeit with a very large dispersion of estimated ages (i.e. 8-220 Myr; R. J. De Rosa et al. 2014; T. J. David & L. A. Hillenbrand 2015).

Table 1 lists the star’s properties, derived either from the literature or from our analysis below. We use empirical comparisons to stars with well-constrained ages to provide a context for HIP 71618’s likely age. Its *Gaia* color-magnitude diagram position is consistent with those of stars in the Pleiades (~ 115 Myr), κ And ($t \sim 47$ Myr), β Pic ($t \sim 24$ Myr) and other young

field stars with interferometrically-determined of ages less than 150 Myr, while it lies closer to the Pleiades sequence than HIP 99770 ($t \sim 115\text{-}200$ Myr) and far closer than stars in the 414 Myr-old Ursa Majoris moving group (J. Jones et al. 2016; T. Currie et al. 2023b, Figure 1). Ages less than 20 Myr are arguably disfavored since HIP 71618 is not a known member of any known cluster. We thus nominally adopt an age of 115_{-95}^{+95} Myr, where the lower bounds are set by its lack of membership in a known moving group and upper bounds set by its youth relative to HIP 99770. From the relationship mapping between stellar mass, spectral type, and bolometric correction for a star on the main sequence (M. J. Pecaut & E. E. Mamajek 2013), we favor a stellar mass of $2.05 M_{\odot}$, temperature of $9300 K$ and luminosity of $\log(L_{\text{bol}}/L_{\odot}) = 1.327$.

Previous AO observations did not identify a candidate imaged companion (R. J. De Rosa et al. 2011, 2014), although they identify a candidate ROSAT x-ray source coincident with the star. The star was not observed before with extreme AO platforms (e.g., the Gemini Planet Imager).

The Hipparcos-Gaia Catalog of Accelerations identifies HIP 71618 as having a proper motion anomaly of $\chi^2 = 9.42$ or $\sim 2.61\sigma$ for two degrees of freedom (T. D. Brandt 2021). Similarly, the *Gaia eDR3* astrometric catalogue from P. Kervella et al. (2022) identifies a $\sim 2.7\text{-}\sigma$ significant astrometric acceleration²⁷. The acceleration derived from HGCA is consistent with a substellar companion at $0''.5$ ($0''.25$) with a minimum mass of $\approx 60 M_{\text{Jup}}$ ($22 M_{\text{Jup}}$). Thus, we targeted this star with OASIS survey (PI T. Currie; M. El Morsy et al. 2024).

3. DATA

3.1. Observation and Data Reduction

We observed HIP 71618 in five epochs between 2024 February and 2025 May using the Subaru and Keck telescopes located at Maunakea (see Table 2). At Subaru, the facility AO systems – AO188 in 2024 and AO3K in 2025 – performed the initial correction of atmospheric turbulence (Y. Minowa et al. 2010; J. Lozi et al. 2022). SCEXAO then performed higher-order wavefront error correction and sent the light to the CHARIS integral field spectrograph (IFS) (T. D. Groff et al. 2016). For Keck, we obtained NIRC2 imaging in the L_p broadband filter ($\lambda_o = 3.78 \mu\text{m}$) behind Keck II’s facility Shack-Hartmann AO system.

²⁷ The Gaia eDR3 catalogue identifies HIP 71618 as having a moderately-high Renormalized Unit Weight Error that may also indicate evidence for a companion, but this property did not originally motivate our targeting of the star.

Table 1. Properties of HIP 71618

Property	Value	Refs
$\alpha_{2000.0}$	14:38:50.2	1
$\delta_{2000.0}$	+44:24:16.21	1
Distance (pc)	58.19 ± 0.51	1
π (mas)	17.1844 ± 0.1516	1
$\mu_{\alpha}, \mu_{\delta}$ H-G ^a (mas/yr)	$-68.287 \pm 0.015, -18.122 \pm 0.015$	2
$\mu_{\alpha}, \mu_{\delta}$ G ^b (mas/yr)	$-67.847 \pm 0.174, -18.424 \pm 0.190$	2
$\mu_{\alpha}, \mu_{\delta}$ H ^c (mas/yr)	$-68.218 \pm 0.506, -18.700 \pm 0.440$	2
Proper Motion Anomaly	$\chi^2=9.421, 2.612\sigma$	2
Mass (M_{\odot})	$2.05_{-0.07}^{+0.13}$	3
Spectral Type	A1V	4
T_{eff} (K)	9300_{-500}^{+400}	3
$\log(L_{\text{bol}}/L_{\odot})$ (dex)	1.327 ± 0.029	3
Angular Diameter (mas)	0.291 ± 0.0151	5
V (mag)	5.387 ± 0.009	6

NOTE—References: (1) - Gaia Collaboration et al. (2023), (2) - T. D. Brandt (2021), (3) - M. J. Pecaut & E. E. Mamajek (2013)/this work, (4) - M. Wenger et al. (2000a), (5) - P. Kervella et al. (2022), (6) - M. Wenger et al. (2000b). a,b,c - proper motion measurements drawn from the Hipparcos-Gaia scaled positional distance (H-G), Gaia eDR3 (G), and Hipparcos (H) in T. D. Brandt (2021).

For the 2025 March SCEXAO/CHARIS observations, the seeing was extremely poor (up to $3''$ seeing), yet AO3K+SCEXAO was able to sustain an AO correction and usually produce a dark hole. The 2024 June Keck data were obtained through highly variable clouds. Otherwise, seeing conditions were slightly below average for Maunakea and photometric. All data were acquired in pupil-tracking mode, allowing the sky to rotate relative to the detector and thus enabling angular differential imaging (ADI; C. Marois et al. 2006), with integration times of 7.5–88 minutes.

SCEXAO/CHARIS data use a Lyot coronagraph with a $0''.113$ focal plane mask to suppress starlight. All CHARIS data were recorded in low spectral resolution/“broadband” mode covering the JHK passbands simultaneously ($\lambda = 1.15\text{--}2.39 \mu\text{m}$, $R \sim 18$). For image registration and spectrophotometric calibration, we modulated the SCEXAO deformable mirror (DM) to produce satellite spots $\sim 16 \lambda/D$ from the star (N. Jovanovic et al. 2015).

We extracted the CHARIS data cubes within the Automated Data Extraction, Processing, and Tracking System (ADEPTS) (2024 data, T. L. Tobin et al. 2020, 2022) or independently with identical settings (2025

Table 2. HIP 71618 Observing Log

UT Date	Instrument	Seeing ^c (")	Filter	λ (μm) ^a	t_{exp}	N_{exp}	ΔPA ($^{\circ}$)	SNR ^d
20240220	AO188+SCExAO/CHARIS	0.7	<i>JHK</i>	1.15-2.37	25.08	88	41.1	84.1
20240223	Keck/NIRC2	0.7	L_p	3.78	30	85	27.19	9.1
20240617	Keck/NIRC2	0.7	L_p	3.78	30	43	50.59	15.8
20250314	AO3K+SCExAO/CHARIS	1-3	<i>JHK</i>	1.15-2.37	20.65	257	52.38	27.6
20250512	AO3K+SCExAO/CHARIS	0.6	<i>JHK</i>	1.15-2.37	25.08	18	5.06	26.6 ^b

NOTE— a) For CHARIS data, the $\lambda_{\mu\text{m}}$ column refers to the wavelength range. For NIRC2 imaging data, it refers to the central wavelength. b) Reduced with SDI only: extracted spectrum is less reliable.

data), following [T. D. Brandt et al. \(2017\)](#). We further processed data with the CHARIS data processing pipeline ([T. Currie et al. 2020b](#)) as in previous work ([T. Currie et al. 2023b](#); [T. L. Tobin et al. 2024](#)). Key reduction steps include sky subtraction, image registration, spectrophotometric calibration, PSF subtraction, and spectral extraction. For spectrophotometric calibration, we used a Kurucz model atmosphere ([F. Castelli & R. L. Kurucz 2003](#)) appropriate for an A1V star.

For the February 2024 and May 2025 data sets, HIP 71618 B was visible in the raw, quicklook CHARIS images produced in real time. Thus, our PSF subtraction approach used rather conservative settings with the adaptive locally optimized combination of images (A-LOCI) algorithm ([T. Currie et al. 2012, 2015](#)) minimizing signal loss, applying a pixel mask over the subtraction zone ([C. Marois et al. 2010](#); [T. Currie et al. 2012](#)) and constructing a reference PSF to minimize residuals within the surrounding optimization region ([D. Lafrenière et al. 2007](#)). For the 2024 February and 2025 March data, we performed PSF subtraction using ADI only, using rotation gaps of $\delta = 1.5$ and 0.75 , respectively (see [D. Lafrenière et al. 2007](#)). The 2025 May data covered a very small parallactic angle motion, so we performed these data using spectral differential imaging (SDI; [C. Marois et al. 2000](#); [W. B. Sparks & H. C. Ford 2002](#)) with a radial scaling gap of $\delta = 1$.

We reduced the NIRC2 data using the ADI-based pipeline from [T. Currie et al. \(2011\)](#), following reduction steps as described in [M. El Morsy et al. \(2025\)](#). Because HIP 71618 B is a more challenging detection for NIRC2, our PSF subtraction settings are slightly more aggressive, consistently using a smaller rotation gap threshold of $\delta = 0.75$ and no pixel mask over the subtraction zone.

3.2. Detections, Spectra, and Astrometry

Figure 2 shows the detection of HIP 71618 B at roughly the 2 o'clock position $\approx 0''.3$ from the star. Adopting the standard definition for signal-to-noise ra-

tio (SNR) (e.g. [T. Currie et al. 2011](#)) – corrected for finite sample sizes as in [D. Mawet et al. \(2014\)](#) – HIP 71618 B is visible at SNR = 26-81 in the CHARIS data sets and SNR = 9.1–15.8 with NIRC2. Comparing the earliest and latest CHARIS images suggests a slight decrease in HIP 71618 B’s projected separation.

To correct for spectrophotometric and astrometric biases in the SCExAO/CHARIS data introduced by PSF subtraction, we apply forward modeling described in [T. Currie et al. \(2018\)](#). To empirically estimate astrometric uncertainties, we adopt the approach described in [M. Kuzuhara et al. \(2022\)](#): we inject a forward-model PSF at the same angular separation as the object but we vary the azimuthal angle. We then compare the input and recovered centroid positions in pixels for an empirical estimate of the centroiding uncertainty, which we then combine quadratically with the stellar centroid uncertainty. Finally, we convert our astrometry to polar coordinates: the final astrometric error budget considers the centroiding uncertainty, the uncertainty in the star’s position (set at 0.25 pixels), and the uncertainty in the north position angle and pixel scale.

Our CHARIS spectrum extracted from the 2024 February epoch is listed in Table 3; relative astrometric positions and uncertainties are listed in Table 4, where the table caption lists our adopted astrometric calibration. The spectrum extracted from March 2025 is noisier but otherwise agrees with the February 2024 spectrum within $1\text{-}\sigma$ errors. Calibrating HIP 71618 B’s spectrum from the May 2025 data is more challenging because it was processed with SDI (see [L. Pueyo et al. 2012](#); [L. Pueyo 2016](#)). Thus, we focus on the 2024 February CHARIS data and NIRC2 data for atmospheric analysis.

We calculate the spectral covariance matrix following the parameterization in [J. P. Greco & T. D. Brandt \(2016\)](#). We find a best-fitting model of $A_\rho = 0.2164$, $A_\lambda = 0.5745$, $A_\sigma = 0.2091$, $\sigma_\rho = 0.4309$, and $\sigma_\lambda = 0.4585$ (see [J. P. Greco & T. D. Brandt 2016](#), for de-

tails). Thus, spectrally correlated noise dominates the residual speckle properties.

From CHARIS, we then estimate photometry of $J, H, K_s = 13.58 \pm 0.06, 13.10 \pm 0.05,$ and 12.78 ± 0.09 . For NIRC2, variable clouds preclude a precise photometric calibration from the 2024 June epoch, while our 2024 February data yield $m_{L_p} = 12.27 \pm 0.19$.

Table 3. HIP 71618 B Spectrum Extracted from February 2024 CHARIS Data

Wavelength (μm)	F_ν (mJy)	σF_ν (mJy)	SNR
1.160	5.441	0.750	28.7
1.200	5.551	0.486	25.9
1.241	5.268	0.284	31.1
1.284	6.124	0.306	41.1
1.329	5.498	0.272	41.2
1.375	3.761	0.194	32.1
1.422	4.300	0.212	33.1
1.471	4.648	0.201	45.5
1.522	5.067	0.240	34.1
1.575	5.663	0.277	35.1
1.630	6.429	0.347	27.1
1.686	6.632	0.332	33.0
1.744	6.091	0.351	24.2
1.805	4.455	0.411	23.6
1.867	4.962	0.294	24.3
1.932	5.110	0.273	35.1
1.999	4.501	0.270	35.0
2.068	5.078	0.383	25.8
2.139	5.333	0.354	29.6
2.213	5.290	0.518	20.1
2.290	5.347	0.505	20.5
2.369	3.277	0.936	18.8

Table 4. HIP 71618 B Astrometry

UT Date	Instrument	Filter	ρ ''	PA (deg)
20240220	SCEXAO/CHARIS	<i>JHK</i>	0.311 ± 0.003	297.896 ± 0.601
20240223	Keck/NIRC2	L_p	0.304 ± 0.009	298.282 ± 0.380
20240624	Keck/NIRC2	L_p	0.303 ± 0.004	297.038 ± 0.377
20250314	SCEXAO/CHARIS	<i>JHK</i>	0.295 ± 0.004	297.634 ± 0.625
20250512	SCEXAO/CHARIS	<i>JHK</i>	0.289 ± 0.006	297.343 ± 0.647

NOTE—We adopt a pixel scale and north position angle offset of 16.10 ± 0.04 mas pixel $^{-1}$, $-2.03 \pm 0.27^\circ$ for CHARIS and 9.971 ± 0.004 mas pixel $^{-1}$, $0.262 \pm 0.020^\circ$ for NIRC2 (T. Currie et al. 2025; M. Service et al. 2016). Using the older CHARIS astrometric calibration from T. Currie et al. (2018, 2022) instead yields almost identical results for our dynamical modeling.

4. ATMOSPHERE ANALYSIS

4.1. Empirical Constraints on HIP 71618 B’s Atmosphere

We compare the JHK band spectra of HIP 71618 B from the February 2024 SCEXAO/CHARIS observation with MLT substellar objects from the Montreal Spectral Library (J. Gagné et al. 2015), using Equation 7 from T. Currie et al. (2018) to quantify the goodness-of-fit, considering both the spectroscopic errors and the spectral covariance.

HIP 71618 B is best fit by the low-gravity M6 dwarf 2MASSJ0318-3708 (Figure 3; $\chi_\nu^2 \sim 1.4$). While low-gravity M6 dwarfs do not have effective temperatures listed in M. J. Pecaut & E. E. Mamajek (2013), their older field counterparts have temperatures of ~ 2800 K: young, low-gravity mid M dwarfs (i.e. M4–M5) have temperatures ≈ 40 – 170 K cooler. The full range of spectral types yielding comparable fit qualities ($\chi_\nu^2 \sim 1.4$ – 2) is dominated by M6–M8 intermediate- and low-gravity dwarfs (< 2570 – 2800 K) with a few M7–M9 field dwarfs (2450 – 2650 K). Thus, empirical comparisons favor HIP 71618 B as an M6–M8 low-to-intermediate-gravity dwarf with a temperature of ≈ 2600 – 2800 K or less.

4.2. Atmospheric Model Comparisons

We use the solar metallicity BT-Settl model grid to further explore HIP 71618 B’s atmosphere (F. Allard et al. 2012), covering temperatures and gravities of 400–4000 K and $\log(g) = 3$ – 5.5 , respectively, and adopting chemical abundances from M. Asplund et al. (2009). The models assume chemical equilibrium and include the effects of dust opacity and a cloud model. Following T. Currie et al. (2023a), we identify the radius for each model that minimizes the χ^2 statistic for fitting our SCEXAO/CHARIS JHK spectrum and the NIRC2 photometric point. We assume a distance of 58.2 pc when performing the comparison.

The best-fitting BT-Settl model has a temperature of 2700 K, a gravity of $\log(g) = 4.5$, and a radius of $1.696 R_{\text{Jup}}$ ($\chi_\nu^2 = 1.677$) (Figure 3, top panel). Figure 3, bottom panel shows $\Delta\chi^2$ contours in the T_{eff} – $\log(g)$ plane for the BT-Settl model fit. While the surface gravity is poorly constrained, the 1σ and 2σ contours correspond to narrower ranges in temperatures of ~ 2650 – 2800 K and ~ 2600 – 2850 K, respectively.

From the best-fitting BT-Settl model, we estimate HIP 71618 B’s luminosity to be $L = 5.54 \times 10^{23}$ W, or $\log\left(\frac{L}{L_\odot}\right) \approx -2.84$. This luminosity is slightly higher than typical luminosities of old field M6–M8 dwarfs listed in M. J. Pecaut & E. E. Mamajek (2013), which have luminosities of $\log\left(\frac{L}{L_\odot}\right) \sim -2.98$ to -3.28 . Adopt-

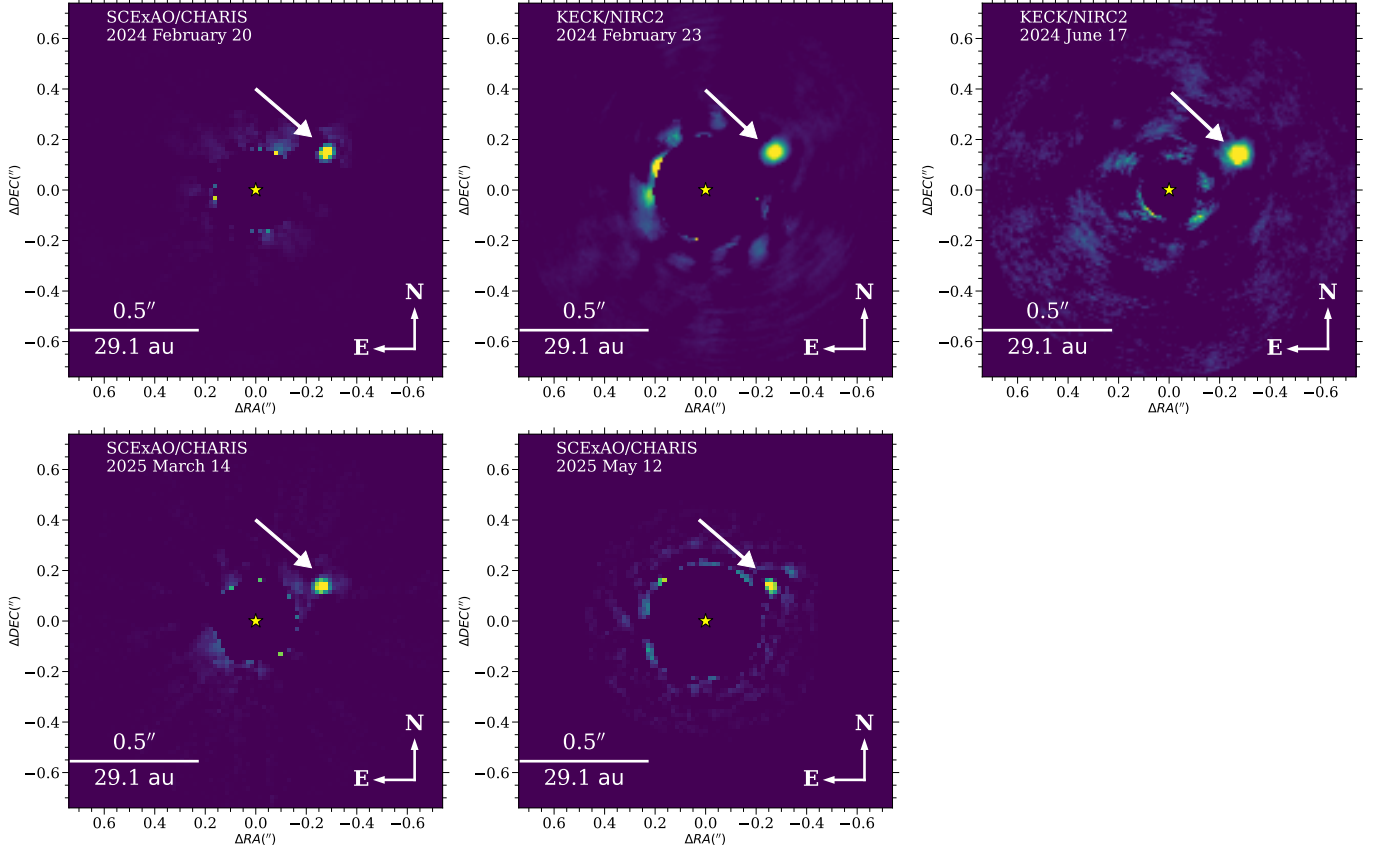


Figure 2. Wavelength-collapsed images of HIP 71618 B with SCExAO/CHARIS in broadband near-infrared light ($1.15\text{--}2.37\ \mu\text{m}$) and with Keck/NIRC2 in the L_p filter ($3.78\ \mu\text{m}$). The white arrow denotes the position of HIP 71618 B in each panel.

ing an age range of 20–200 Myr and assuming the COND evolutionary models to convert from luminosity to mass (I. Baraffe et al. 2003), HIP 71618 B’s luminosity is consistent with a $30\text{--}100\ M_{\text{Jup}}$ companion.

5. DYNAMICAL MODELING

We constrained the dynamical mass of HIP 71618 B and its six Keplerian orbital parameters using the open-source Markov Chain Monte Carlo (MCMC) code *orvara* (T. D. Brandt 2021), combining absolute astrometry from HGCA (T. D. Brandt 2021) with relative astrometry from SCExAO/CHARIS and Keck/NIRC2, as listed in Table 4. Consistent with the primary’s spectral type (see M. J. Pecaut & E. E. Mamajek 2013), we adopted a prior of $2.05 \pm 0.25\ M_{\odot}$ for the host star and use the *Gaia* *eDR3* parallax and uncertainties to define a prior on the parallax.

We carried out two separate fits, which differ in terms of the companion mass prior: (1) assuming a gaussian prior centered on $65\ M_{\text{Jup}}$ with a standard deviation of $35\ M_{\text{Jup}}$ and (2) a flat prior for the companion mass, as

in T. Currie et al. (2023b)²⁸. The gaussian prior encompasses most of the luminosity-inferred mass range described in the previous section, with a slight bias against masses $<30\ M_{\text{Jup}}$, which are most consistent with ages less than 20 Myr. Each *orvara* simulation consists of 100 walkers per temperature, 20 temperatures, 200,000 steps per walker, and thinned the chains by a factor of 50. The first 100 steps of the thinned chain are treated as burn-in.

Table 5 summarizes adopted priors for these two simulations and fitted parameters. Figure 4 displays the orbital parameter posterior distributions and an ensemble of orbital solutions for the gaussian prior case. Both

²⁸ Most of our prior work considered a log-uniform prior (*orvara*’s default option) and a flat prior (e.g. T. Currie et al. 2023a, 2025; D. Bovie et al. 2025). However, adopting a true log-uniform prior causes a pile-up of solutions near unphysically low masses, where the prior has the highest probability density. This numerical artifact is due to HIP 71618 B’s relatively noisy astrometric acceleration measurement combined with a lack of evidence for orbital curvature. HIP 99770 b has a similarly noisy acceleration measurement but does not suffer this artifact due to its more face-on orbit and larger angular displacement with time.

Table 5. MCMC Orbit Fitting Results

Parameter	16/50/84% quantiles	Prior
Fitted Parameters (1,2) ^a		
RV jitter (m/s)	0.14 ⁺⁵⁷ _{-0.14} , 0.10 ⁺⁵³ _{-0.10}	log-uniform
$M_{\text{pri}} (M_{\odot})$	2.07 ^{+0.24} _{-0.24} , 2.07 ^{+0.25} _{-0.25}	Gaussian, 2.05 ± 0.25
$M_{\text{sec}} (M_{\text{Jup}})$	60 ⁺²⁷ ₋₂₁ , 65 ⁺⁵⁴ ₋₂₉	$65 \pm 35 M_{\text{Jup}}$ (1-gaussian) ^a , $1/M_{\text{sec}}$ (2-flat/uniform) ^a
Semimajor axis a (au)	11.1 ^{+1.3} _{-1.0} , 11.3 ^{+1.3} _{-1.0}	$1/a$ (log-uniform)
$\sqrt{e} \sin \omega^*$	0.02 ^{+0.42} _{-0.43} , 0.02 ^{+0.46} _{-0.45}	uniform
$\sqrt{e} \cos \omega^*$	0.73 ^{+0.18} _{-1.6} , -0.57 ^{+1.5} _{-0.31}	uniform
Inclination ($^{\circ}$)	98 ⁺²⁰ ₋₁₀ , 97 ⁺¹⁸ ₋₁₁	$\sin i$ (geometric)
PA of the ascending node Ω ($^{\circ}$)	122.5 ⁺¹⁷⁶ _{-6.2} , 286 ⁺¹⁵ ₋₁₆₉	uniform
Mean longitude at 2010.0 ($^{\circ}$)	104 ⁺¹⁴¹ ₋₇₇ , 189 ⁺⁵⁹ ₋₁₄₉	uniform
Parallax (mas)	17.18 ^{+0.12} _{-0.12} , 17.18 ^{+0.12} _{-0.12}	Gaussian, 0
Derived Parameters(1,2) ^a		
Period (yrs)	25.6 ^{+4.4} _{-3.1} , 26.0 ^{+4.0} _{-3.2}	
Argument of periastron ω ($^{\circ}$)	176 ⁺¹⁶⁴ ₋₁₅₆ , 178 ⁺¹⁵¹ ₋₁₄₈	
Eccentricity e	0.87 ^{+0.10} _{-0.22} , 0.898 ^{+0.086} _{-0.22}	
Semimajor axis (mas)	191 ⁺²³ ₋₁₇ , 193 ⁺²² ₋₁₇	
Periastron time T_0 (JD)	2463402 ⁺¹¹¹¹ ₋₇₅₀₉ , 2463390 ⁺¹⁰⁵² ₋₇₂₀₇	
Mass ratio	0.028 ^{+0.013} _{-0.010} , 0.030 ^{+0.027} _{-0.014}	
Predicted Locations (1,2) ^a		
2027.0	0''261 \pm 0.009, 296.444 \pm 1.600 $^{\circ}$, 0''261 \pm 0.009, 296.884 \pm 1.620 $^{\circ}$	
2027.5	0''247 \pm 0.010, 296.044 \pm 2.047 $^{\circ}$, 0''248 \pm 0.013, 296.914 \pm 2.286 $^{\circ}$	

^a Quantiles listed are for the simulations assuming 1) a gaussian companion mass prior centered on $65 M_{\text{Jup}}$ and 2) a flat prior.

simulations favor a semimajor axis of ~ 11 au: 11.2^{+1.4}_{-1.1} and 11.3^{+1.3}_{-1.2} for the gaussian prior and flat companion mass prior simulations, respectively. Both simulations also favor an orbit viewed nearly edge-on (96⁺¹⁸₋₁₀ and 95⁺¹⁹₋₁₂).

Our simulations find a broad eccentricity distribution favoring very high values (0.87^{+0.11}_{-0.23} for the gaussian prior, 0.90^{+0.08}_{-0.22} for the flat prior). Other bound substellar companions likewise have broad eccentricity posteriors favoring high values, especially when a very small fraction of the companion's orbit is sampled (B. P. Bowler et al. 2020; S. Blunt et al. 2023). Examining the posterior chains shows that HIP 71618 B's Hipparcos measurement likely favors a higher eccentricity, while other parameters show no preference. To further test this hypothesis, we reran *orvara* with the HGCA astrometry turned off. The resulting posterior distribution recovered our nominal results for primary mass, semimajor axis, and inclination, albeit with much larger errors. However, it found less preference for a very high eccentricity ($e \sim 0.67$ ^{+0.29}_{-0.41}).

For both the gaussian and flat prior simulations, the median and nearly all of the 68% confidence interval lie below the hydrogen limit ($\approx 78.5 M_{\text{Jup}}$; G. Chabrier et al. 2023) – 60⁺²⁷₋₂₁ M_{Jup} and 65⁺⁵⁴₋₂₉ M_{Jup} – thus favoring a brown dwarf interpretation for HIP 71618 B. The corresponding mass ratio is low for a brown dwarf com-

panion, just barely above the empirical turnover in mass ratios between brown dwarfs and planets identified from large ensembles of substellar objects ($q \sim 0.028$ ^{+0.013}_{-0.010} and $q \sim 0.030$ ^{+0.027}_{-0.014} for a gaussian and flat companion mass prior, respectively) (T. Currie et al. 2023b, 2025)²⁹.

Given HIP 71618 B's luminosity and adopting the COND luminosity evolution models, the companion's dynamical mass is consistent with an object with an age between 15 Myr and 150 Myr (gaussian prior) or >15 Myr (flat prior), where HIP 71618 B's median posterior mass is most consistent with a ≈ 60 -70 Myr-old object. The COND models predict that an object with HIP 71618 B's luminosity lies below the hydrogen-burning limit if the age is $\lesssim 110$ Myr – i.e. if the age is roughly that of the Pleiades or less.

An age equal to or slightly younger than the Pleiades thus provides a self-consistent interpretation of HIP 71618 B's given its dynamical mass and luminosity, adopting the COND evolutionary model framework. However, masses inferred from luminosity evolution models can show conflicts with precise dynamical masses (T. J. Dupuy et al. 2014); different luminosity evolution

²⁹ We find similar results for an *orvara* simulation using a log-uniform prior but removing artificially low companion mass solutions from the Markov chains: 46⁺³⁸₋₂₂ M_{Jup} .

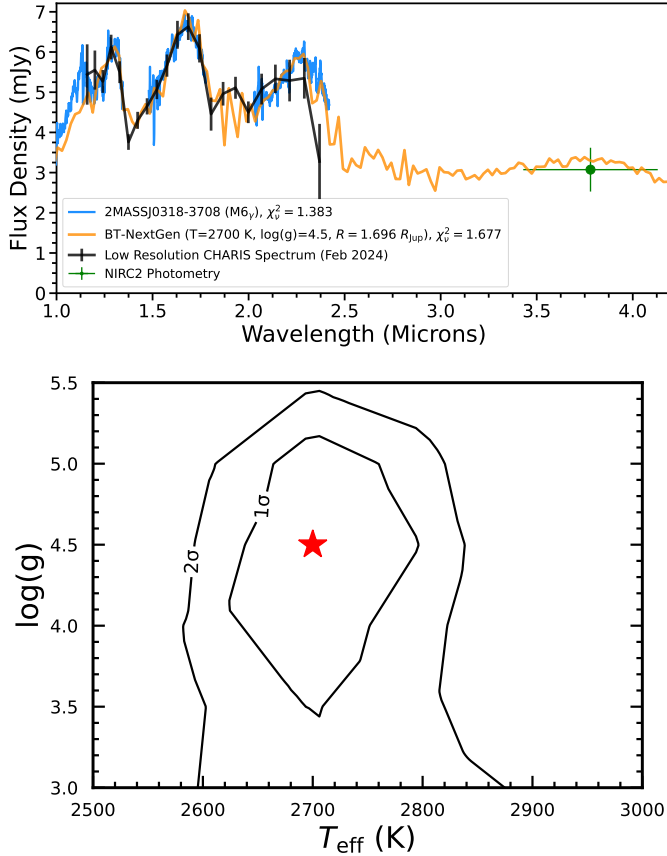


Figure 3. (Top) HIP 71818 b data compared to the best-fit model from the BT-Settl grids in the near-IR spectrum and NIRC2 datapoint. (Bottom) Contour plot showing the confidence intervals for the BT-Settl model grid. The red star indicates the best-fit.

models can yield different mappings between luminosity, mass, and age (e.g. G. M. Brandt et al. 2021).

6. HIP 71618 B: A TARGET FOR THE ROMAN CORONAGRAPH INSTRUMENT TECHNOLOGY DEMONSTRATION

HIP 71618 B is a ~ 2600 – 2800 K companion to a bright primary ($V \sim 5.4$) at a projected separation of $\approx 0''.3$. The Roman Coronagraph Instrument is predicted to yield deep ($\sim 10^{-9}$ – 10^{-8}) contrasts at 575 nm over $0''.15$ – $0''.45$. It has a single Threshold Technical Requirement (TTR5) for success³⁰: achieve a $5\text{-}\sigma$ contrast better than 10^{-7} at $\lambda_c \leq 600$ nm ($>10\%$ bandpass) located 6 – $9 \lambda/D$ ($\sim 0''.3$ – $0''.45$) from a bright ($V_{AB} \leq 5$) star in under 10

³⁰ https://roman.gsfc.nasa.gov/science/rsig/2021/Roman-Requirements_20201105.pdf

hr³¹. The Roman Coronagraph passband available for TTR5 is centered on 575 nm.

Here, we consider whether HIP 71618 is suitable for demonstrating TTR5. We emphasize that this statement is *not* equivalent to “HIP 71618 is the *only* system that can demonstrate TTR5”. Other suitable systems – companionless stars or newly discovered systems with imaged companions – assuredly exist. However, they must be demonstrated from future analyses *in peer-reviewed studies* before they can be properly considered.

6.1. HIP 71618 B Will Lie Within The Roman Coronagraph Dark Hole Region

We first predict HIP 71618 B’s position during the technology demonstration phase from our best-fitting orvara orbits. We assume that this phase occurs during the first six months of full Roman Coronagraph operations in January – July 2027, assuming a launch date of October 2026 and three months of commissioning time. During this timeframe, HIP 71618 B should lie at $\rho \sim 0''.26 \pm 0''.01$ in January 2027 and $0''.25 \pm 0''.01$ in July 2027 (~ 5 – $5.2 \lambda/D$) from the star (Figure 5, top panel), well within the $0''.15$ – $0''.45$ dark hole region where the latest full coronagraph simulation (OS 11) and TVAC tests predict an approximately flat 5σ contrast floor of $\approx 2 \times 10^{-8}$ or lower.

6.2. HIP 71618 Has Plausible PSF Reference Stars

Roman Coronagraph observations of HIP 71618 require suitable reference stars for digging dark holes, which the Roman Coronagraph Community Participation Program (CPP) team is now vetting (S. G. Wolff et al. 2024). From the CPP spreadsheet of candidate PSF reference stars³², we identified HD 120315 – flagged as “good?” through 2025 August 1 and as “B” no later than 2025 September 1 – as a plausible reference. It is located 10 degrees from HIP 71618³³. Additionally, we used the *SIMBAD* database to search for other very bright stars ($V \lesssim 3$ – 3.5) close to HIP 71618 in the sky

³¹ By construction, demonstrating the 10^{-7} contrast threshold in more challenging configurations – e.g. on a star slightly fainter than $V = 5$ or on a companion located between 3 and $6 \lambda/D$ – would also fulfill TTR5.

³² <https://docs.google.com/spreadsheets/d/1p5r0VmjBCjXU25daJl5oJOPoPh1V79nuESbnwmca0s0/edit?usp=sharing>

³³ The deepest publicly available data for HD 120315 are Keck/NIRC2 data obtained in 2014. Through at least 2025 August 1, the Roman CPP team listed HD 120315 as “data reduction in progress”. We processed these data and did not identify a stellar companion that would preclude the star from being a suitable PSF reference.

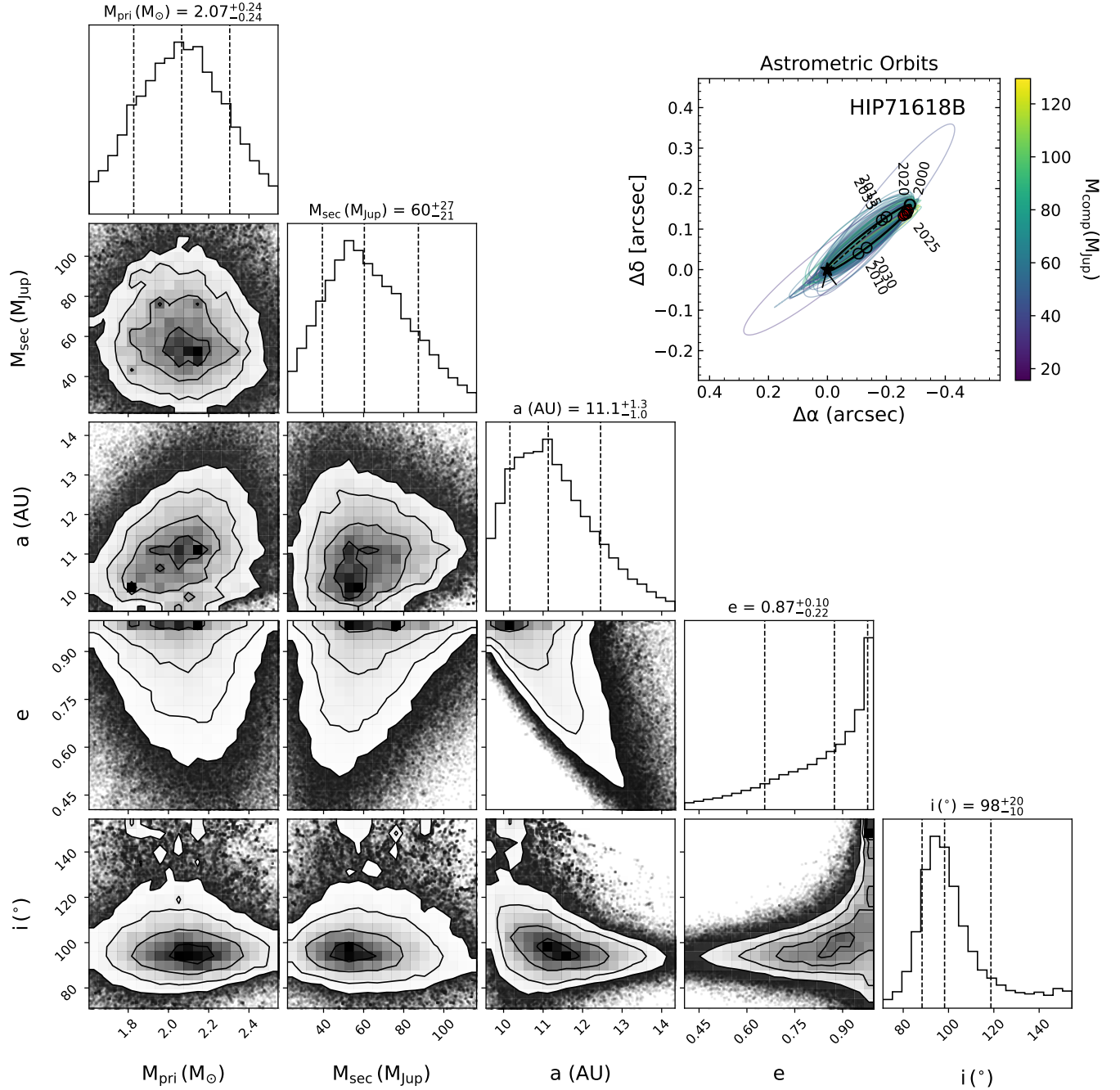


Figure 4. Corner plot showing posterior distributions of selected orbital parameters from jointly modeling direct imaging and astrometric data assuming a gaussian companion mass prior centered on $65 M_{\text{Jup}}$. The contour lines delineate the regions encompassing 68, 95, and 99% of the posteriors. The corner plot for the simulation adopting a flat companion mass prior is very similar except that its long tail of higher mass solutions results in a slightly larger range of masses within the 68% confidence interval.

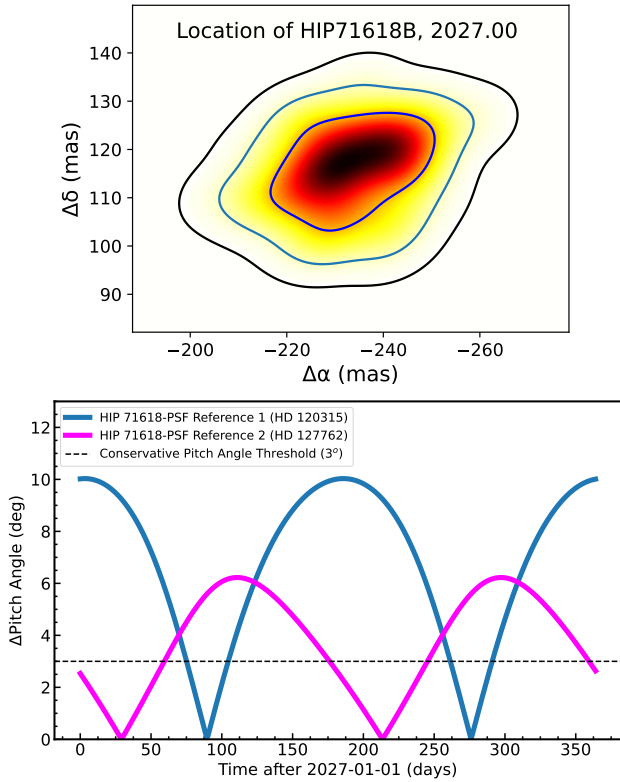


Figure 5. (top) Predicted location of HIP 71618 B in 2027 January from the *orvara* dynamical modeling results presented in Table 5, assuming a gaussian companion mass prior. (bottom) The pitch angle difference between HIP 71618 and two potential reference stars for dark-hole digging in 2027 with the conservative pitch angle threshold displayed as a dashed line.

that are plausible PSF references despite not being on the CPP’s spreadsheet. This search identifies at least one additional candidate PSF reference star, HD 127762 (A7IV), which lies within 6° of HIP 71618, lacks a bright known companion from optical interferometric data, and has an angular diameter below the 2 mas threshold for inclusion ($\theta_{\text{diameter}} \sim 1.77$ mas) (E. K. Baines et al. 2023). It was likely missed due to its *Simbad*-listed V band magnitude being just 0.02 mag fainter than the nominal CPP cutoff ($V = 3.02$).

The instrument’s thermal stability limits its performance. Differences in the pitch angle greater than 3° between the telescope pointing to a target vs. PSF reference and the Sun may degrade contrasts. However, for over 90% of a calendar year, HIP 71618’s pitch angle is within 3° of at least one of the two aforementioned PSF stars (Fig. 5, bottom panel).

A TTR5-achieving observation of HIP 71618 can be efficiently scheduled. HIP 71618 and HD 102315 both

have ecliptic longitudes $> 54^\circ$ and are thus in or very close to the Roman Continuous Viewing Zone (CVZ, B. Rose et al. 2023), enabling highly flexible scheduling, while HD 127762 is very close to the CVZ. Keepout maps generated for HIP 71618 and its two candidate PSF references³⁴ identifying non-scheduleable epochs show that HIP 71618 and HD 102315 can be imaged by Roman year-round in 2027, while HD 127762 is observable except for two ~ 40 -day blocks (70–110 and 260–310 days after January 1).

6.3. A High Signal-to-Noise Ratio Detection Of HIP 71618 B With The Roman Coronagraph Would Fulfill The Instrument’s Core Technology Demonstration Goal

To estimate HIP 71618 B’s contrast at 575 nm and other passbands, we use predicted contrasts from the B. Lacy & A. Burrows and BT-Settl/BT-NextGen atmosphere models and compare these results to empirical spectra and photometry for field dwarfs and younger, lower gravity dwarfs. For the B. Lacy & A. Burrows models, we focus on temperatures of 2600–2800 K and a gravities of $\log(g)=4\text{--}5$ and the radii for each temperature/gravity combination that minimizes the χ^2 value. These models incorporate new line lists particularly relevant for the Roman Coronagraph passbands (see T. Currie et al. 2023b; D. Bovie et al. 2025). For the older BT-Settl/NextGen models, we focus on the best-fitting model phase space (temperature, gravity, radius) found in Section 4.2.

For an empirical calibration of HIP 71618 B’s expected contrast, we add optical spectra for young, low-gravity members of the TW Hya and the Tucana-Horologium moving groups (~ 10 Myr and 45 Myr old, respectively) drawn from K. L. Luhman et al. (2017) and K. L. Luhman (2023, 2024): 2MASS J00514561-6227073/Gaia DR3 4710164571939123456 (M5.5-M6), 2MASS J00200551-5359372/Gaia DR3 4923392999353596288 (M7.25), and TWA 26 (M8.5). The spectra do not extend to the near-IR filters where we detect HIP 71618 B. Thus, we normalize these spectra within a 100 nm bandpass centered on 850 nm to the best-matching subset of BT-Settl/NextGen models that fit also HIP 71618 B within $\chi_\nu^2 < 2$. The 700–1000 nm portion of the M5.5-M6, M7.25, and M8.5 standard spectra are best matched by BT-NextGen models of 2800 K/ $\log(g) = 4.5$, 2700 K/ $\log(g) = 4.5$, and 2600 K/ $\log(g) = 4.5$, respectively.

³⁴ These can be easily modifiable from https://github.com/roman-corgi/roman_pointing/blob/main/Notebooks/roman_pointing_demo.ipynb.

Finally, we add measurements of HD 1160 B obtained with SCEXAO/VAMPIRES (B. Norris et al. 2015; M. Lucas et al. 2024). HD 1160 B has a spectral type similar to or slightly earlier than HIP 71618 B, likely has a similar mass, and likely has a comparable age but orbits its host star at a far wider separation making its detection significantly less challenging (E. L. Nielsen et al. 2012; E. V. Garcia et al. 2017). We observed HD 1160 with SCEXAO and the upgraded VAMPIRES detector on 2023 July 11 in excellent seeing conditions in four passbands centered on 614 nm, 670 nm, 720 nm, and 760 nm. The observing sequence covers 17 minutes of integration time and 14 degrees of parallactic angle rotation (~ 10 -12 λ/D at HD 1160 B's separation). The data were reduced using the VAMPIRES Data Processing Pipeline (M. Lucas et al. 2024); we performed PSF subtraction using the GreeDS algorithm (B. Pairet et al. 2021), an improvement upon the widely-used Principal Component Analysis-based subtraction approach (A. Amara & S. P. Quanz 2012; R. Soummer et al. 2012). This approach yielded high SNR detections at 720 and 760 ($\sim 29\sigma$ and 34σ), a weaker detection at 670 nm ($\sim 6.3\sigma$), and a 2.4σ residual at 614 nm consistent with a noisy detection. The throughput-corrected contrasts at 610 nm, 670 nm, 720 nm, and 760 nm are then 1.3×10^{-6} , 3.8×10^{-6} , 1.7×10^{-5} , and 3.0×10^{-5} , respectively. Around HIP 71618, HD 1160 B would have a contrast $\sim 14\%$ fainter in all bands.

Figure 6 shows our results. The Lacy/Burrows models predict 575 nm contrasts of $\sim 5.7 \times 10^{-7}$ from the best-fit temperature and gravity (2700 K, $\log(g) = 4.5$) and 3 - 10×10^{-7} for other models displayed (top panel). The predicted contrasts agree very well with the measured optical contrasts for HD 1160 B (black dots). Thus, assuming these models accurately predict HIP 71618 B's 575 nm brightness, a $\text{SNR} = 28.5$ detection of HIP 71618 B will likely demonstrate a $5\text{-}\sigma$ contrast of 10^{-7} contrast. A $\text{SNR} = 50$ detection would demonstrate this contrast for the upper range of 575 nm contrast predictions.

Contrasts inferred from the optical spectra of young brown dwarfs largely agree with the Lacy/Burrows model predictions (bottom panel). Using the M6 Tuc-Hor standard to guide our estimates, HIP 71618 B should have a contrast of $\sim 1.3 \times 10^{-6}$. The M7.25 and M8.5 standards imply steeper contrasts of $\sim 5.0 \times 10^{-7}$ and 3.1×10^{-7} , respectively: in agreement with model predictions. HD 1160 B's contrasts appear to be in strongest agreement with those from the M7.25 spectral standard. Adopting 575 nm contrast estimates drawn from these standards, a $\text{SNR} = 16$ - 65 detection of HIP

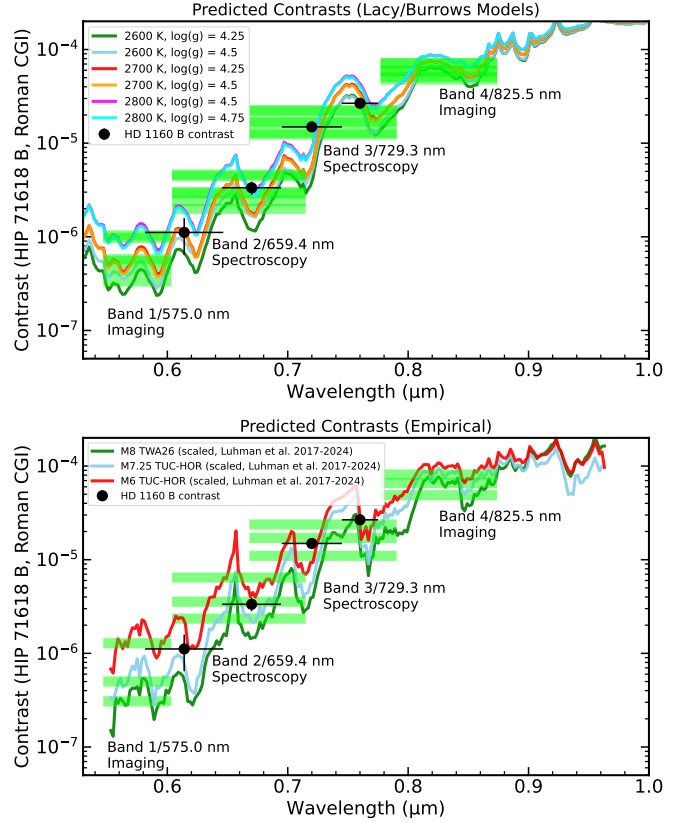


Figure 6. (Top) (top) Predicted contrast for HIP 71618 B in the coronagraph's passbands for different atmosphere models from the updated B. Lacy & A. Burrows (2020) grid distribution. (bottom) Predicted contrasts for HIP 71618 B drawn from flux-normalized optical spectra from the young/low-gravity spectral standards presented in K. L. Luhman et al. (2017) and K. L. Luhman (2023, 2024). The black data points show contrasts for HD 1160 B – a substellar companion with near-IR colors, a mass, and age similar to HIP 71618 B – if it orbited HIP 71618.

71618 B would demonstrate a $5\text{-}\sigma$ contrast of 10^{-7} contrast³⁵.

To estimate the exposure time needed to carry out TTR5-fulfilling coronagraph observations of HIP 71618, we use the Roman Coronagraph Instrument Exposure Time Calculator (Corgi-ETC)³⁶. To achieve 10^{-7} $5\text{-}\sigma$

³⁵ We explored alternate spectral standards drawn from K. L. Luhman et al. (2017) and K. L. Luhman (2023, 2024), especially in the M6–M7 range, but found nearly identical results. While the BT-Settl/NextGen models well reproduce the colors and spectral features of our spectral standards in the red optical, they appear to overpredict the standards' flux densities shortwards of 700 nm. In contrast, they provide excellent fits to spectral of old M dwarfs from the MELCHORS library (P. Royer et al. 2024), hinting at challenges with fitting optical spectra of M dwarfs at low gravities.

³⁶ <https://github.com/roman-corgi/corgietc>

contrasts for HIP 71618 in the optimistic and conservative performance scenarios, Corgi-ETC predicts on-source observing times of 1.5 hrs and 1.75 hrs, respectively, which would yield an $\text{SNR} = 25$ detection of HIP 71618 B for a contrast of 5×10^{-7} . For the worst-case scenario (a 575 nm contrast of $= 3 \times 10^{-7}$), these times only slightly increase (1.9 hrs and 2.5 hrs). Assuming the coronagraph primer observing efficiency estimate (24 hours clock time for 14 hours observing time)³⁷, HIP 71618 observations require nominal clock time of 2.6 hrs and 3 hours for the optimistic and conservative scenarios. Worst-case scenario values are 3.3 hrs and 4.3 hrs. All of these values are well below the time limits specified for TTR5 (10 hours).

Thus, current evidence shows that HIP 71618 is a highly suitable target for demonstrating TTR5 due to its predicted contrast, location, primary brightness, availability of (candidate) PSF reference stars, and ease of scheduling. Follow-up deep high-contrast imaging observations of both stars could confirm the suitability of PSF reference stars.

7. SUMMARY

Our study further demonstrates the utility of programs like OASIS that combine direct imaging and precision astrometry to discover substellar companions. HIP 71618 B likely is a moderate mass brown dwarf ($\approx 60 M_J$) at 11 au but with a mass ratio of $q \approx 0.03$, placing it within the brown dwarf desert where both indirect methods like radial-velocity and direct imaging infrequently find objects (e.g. E. L. Nielsen et al. 2019; A. T. Stevenson et al. 2023; T. Currie et al. 2025). Current data favor a very high eccentricity for HIP 71618 B compared to many other substellar companions detected by imaging and astrometry (e.g. HD 33632 Ab T. Currie et al. 2020a; M. El Morsy et al. 2025), although the eccentricity posterior distribution is quite broad. Early orbital modeling for some substellar objects with relative astrometry covering a short time baseline likewise favored very high eccentricities: subsequent monitoring favored lower eccentricities (e.g. S. Blunt et al. 2023). Further astrometric monitoring and relative RV measurements will enable far better eccentricity constraints, as has been found for HIP 99770 b (D. Bovie et al. 2025; T. O. Winterhalder et al. 2025).

HIP 71618 B could play a unique role in the success of the Roman Coronagraph by being a first target on which to achieve TTR5. HIP 71618 is bright enough ($V = 5.39$) that the instrument should lose little of its nominal

performance (benchmarked at $V \leq 5$). The location of HIP 71618 and potential PSF reference stars within the Roman CVZ significantly relaxes scheduling constraints compared to targets at lower galactic latitudes. A high SNR detection of HIP 71618 B at 575 nm would fulfill TTR5, the instrument’s sole success criterion.

HIP 71618 is especially important because current alternatives for demonstrating TTR5 are, at best, problematic. For example, achieving TTR5 “by analysis” of the residual noise around a companionless star near a PSF reference is possible in principle. However, in this approach, both the PSF reference stars *and* suitable “companionless” star targets must be vetted (e.g. for contaminating binaries at the $\gtrsim 10^{-5}$ level, D. Savransky 2025, pvt. comm.) prior to scheduling consideration. As of October 24 2025 (~ 11 -18 months before launch), there are no publicly announced companionless star vetting programs within the CPP.

A far more striking alternative is to demonstrate TTR5 by reimaging a known, cool substellar companion found from IR high-contrast imaging. However, as has been pointed out many times before (e.g. M. El Morsy et al. 2024), the peer-reviewed literature currently lacks any known imaged companion whose redetection with Band 1 is 1) demonstrated to be likely and 2) would demonstrably fulfill TTR5. E.g. β Pic b is undetectable at 575 nm due to the system’s debris disk. Published models (B. Lacy & A. Burrows 2020) suggest that 51 Eri b is too faint. Updates to these models likewise show HR 8799 e, HD 206893 B, and HIP 99770 b are likely too faint ($\sim 10^{-9}$ – 10^{-11} contrast) (B. Lacy, pvt. comm.; D. Bovie et al. 2025)³⁸. As of October 24 2025, there a dedicated public-facing companion target search within the context of the Roman CPP program, nor is there elsewhere peer-reviewed work from the CPP team clearly demonstrating a sample of suitable imaged companions besides HIP 71618 B.

The suitability of HIP 71618 as a technology demonstration target should motivate timely, deep vetting of reference stars to confirm their lack of binarity at deeper

³⁷ https://roman.ipac.caltech.edu/docs/RomanCoronagraphPrimer_Current.pdf

³⁸ A focus on mature, radial-velocity (RV) detected Jupiter-mass planets only exacerbates target problems. Almost all well characterized, RV-detected mature planets around $V < 5$ stars lie interior to $3\text{--}6 \lambda/D$ for Roman at 575 nm; others require steep contrasts $\lesssim 10^{-9}$ for detection (e.g. v And): only feasible if its current best laboratory contrasts are realized in flight and 100 times more challenging than TTR5’s 10^{-7} contrast threshold. The majority also lack strong orbital constraints in the Exoplanet Imaging Database (due to lack of inclination estimates; resulting uncertainties in time of periastris passage) (D. Savransky, 2025, pvt. comm.). They are not currently considered to be the most straightforward targets for companion detection (D. Savransky, 2025, pvt. comm.).

contrasts. Note that HIP 71618 is $\sim 30\text{-}40\%$ fainter than the nominal target brightness benchmark of $V = 5$, and HIP 71618 B will be located slightly interior to the 6–9 λ/D scoring region but within the region (3–9 λ/D) that both simulations and TVAC tests demonstrate that the coronagraph will yield a deep-contrast dark hole³⁹. Achieving TTR5 on HIP 71618 will therefore present a slightly conservative assessment of the actual instrument performance.

Finally, HIP 71618 B is also well-suited for commissioning observations prior to a TTR5 demonstration and for different purposes. Its modest predicted 730 nm contrast (10^{-5} ; see Figure 5, bottom left panel) suggests it is well suited for long-slit spectroscopy, even if the instrument is not yet tuned well enough to achieve TTR5. Thus, in addition to satisfying TTR5, the system may be well suited for an early demonstration of the instrument’s ability to derive atmospheric properties of sub-stellar objects.

ACKNOWLEDGMENTS

We thank the anonymous referee for timely and helpful suggestions that improved the quality of this paper and Dmitry Savransky for discussions about current Roman CPP target selection preparations. We are extremely grateful to Kevin Luhman for helpful guidance on low-gravity spectral standards and for sharing the TWA 26 spectrum.

The authors acknowledge the very significant cultural role and reverence that the summit of Mauna Kea holds within the Hawaiian community. We are most fortunate to have the opportunity to conduct observations from this mountain.

This work is generously supported by National Science

Foundation (NSF) Astronomy and Astrophysics Grant #2408647 and NASA-Keck Strategic Mission Support Proposal. We are grateful for the continued valuable work and expert guidance of NSF and NASA-Keck personnel, especially in challenging times. M.K. is supported by JSPS KAKENHI (grant No. 24K07108). A.Z. acknowledges support from ANID – Millennium Science Initiative Program – Center Code NCN2024_001 and Fondecyt Regular grant number 1250249.

The development of SCEAO was supported by JSPS (Grant-in-Aid for Research #23340051, #26220704 & #23103002), Astrobiology Center of NINS, Japan, the Mt Cuba Foundation, and the director’s contingency fund at Subaru Telescope. CHARIS was developed under the support by the Grant-in-Aid for Scientific Research on Innovative Areas #2302. SCEAO’s adaptive optics loops and high-speed data acquisition are handled by the CACAO package, which is supported by NSF award 2410616. Some of the data presented herein were obtained at the W. M. Keck Observatory, which is operated as a scientific partnership among the California Institute of Technology, the University of California and the National Aeronautics and Space Administration. The Observatory was made possible by the generous financial support of the W. M. Keck Foundation. Ziying Gu acknowledges the support from the Forefront Physics and Mathematics Program to Drive Transformation (FoPM), a World-leading Innovative Graduate Study (WINGS) Program at the University of Tokyo.

Software: `corgi-etc`: Roman Coronagraph Community Participation Program (CPP)⁴⁰, `roman_pointing`: Roman Coronagraph Community Participation Program (CPP)⁴¹.

REFERENCES

- Allard, F., Homeier, D., & Freytag, B. 2012, *Philos. Trans. R. Soc. Lond., B*, 370, 2765, doi: [10.1098/rsta.2011.0269](https://doi.org/10.1098/rsta.2011.0269)
- Amara, A., & Quanz, S. P. 2012, *MNRAS*, 427, 948, doi: [10.1111/j.1365-2966.2012.21918.x](https://doi.org/10.1111/j.1365-2966.2012.21918.x)
- ³⁹ See demonstrated here https://workshop.ipac.caltech.edu/romanci24/talks/Day1_Poberezhskiy.pdf (page 10, comparing the 3–9 λ/D and 6–9 λ/D performance) and supported here <https://roman.ipac.caltech.edu/page/cgi-contrast-curves.html>
- ⁴⁰ <https://github.com/roman-corgi/corgietc>
- ⁴¹ https://github.com/roman-corgi/roman_pointing/
- Asplund, M., Grevesse, N., Sauval, A. J., & Scott, P. 2009, *ARA&A*, 47, 481, doi: [10.1146/annurev.astro.46.060407.145222](https://doi.org/10.1146/annurev.astro.46.060407.145222)
- Baines, E. K., Clark, III, J. H., Schmitt, H. R., Stone, J. M., & von Braun, K. 2023, *AJ*, 166, 268, doi: [10.3847/1538-3881/ad08be](https://doi.org/10.3847/1538-3881/ad08be)
- Balmer, W. O., Pueyo, L., Stolker, T., et al. 2023, *ApJ*, 956, 99, doi: [10.3847/1538-4357/acf761](https://doi.org/10.3847/1538-4357/acf761)
- Balmer, W. O., Franson, K., Chomez, A., et al. 2025, *AJ*, 169, 30, doi: [10.3847/1538-3881/ad9265](https://doi.org/10.3847/1538-3881/ad9265)
- Baraffe, I., Chabrier, G., Barman, T. S., Allard, F., & Hauschildt, P. H. 2003, *A&A*, 402, 701, doi: [10.1051/0004-6361:20030252](https://doi.org/10.1051/0004-6361:20030252)

- Blunt, S., Balmer, W. O., Wang, J. J., et al. 2023, *AJ*, 166, 257, doi: [10.3847/1538-3881/ad06b7](https://doi.org/10.3847/1538-3881/ad06b7)
- Bovie, D., Currie, T., El Morsy, M., et al. 2025, *AJ*, 170, 254, doi: [10.3847/1538-3881/ae0195](https://doi.org/10.3847/1538-3881/ae0195)
- Bowler, B. P., Blunt, S. C., & Nielsen, E. L. 2020, *AJ*, 159, 63, doi: [10.3847/1538-3881/ab5b11](https://doi.org/10.3847/1538-3881/ab5b11)
- Brandt, G. M., Dupuy, T. J., Li, Y., et al. 2021, *AJ*, 162, 301, doi: [10.3847/1538-3881/ac273e](https://doi.org/10.3847/1538-3881/ac273e)
- Brandt, T. D. 2021, *ApJS*, 254, 42, doi: [10.3847/1538-4365/abf93c](https://doi.org/10.3847/1538-4365/abf93c)
- Brandt, T. D., Dupuy, T. J., & Bowler, B. P. 2019, *AJ*, 158, 140, doi: [10.3847/1538-3881/ab04a8](https://doi.org/10.3847/1538-3881/ab04a8)
- Brandt, T. D., Rizzo, M., Groff, T., et al. 2017, *Journal of Astronomical Telescopes, Instruments, and Systems*, 3, 048002, doi: [10.1117/1.JATIS.3.4.048002](https://doi.org/10.1117/1.JATIS.3.4.048002)
- Castelli, F., & Kurucz, R. L. 2003, in *IAU Symposium*, Vol. 210, *Modelling of Stellar Atmospheres*, ed. N. Piskunov, W. W. Weiss, & D. F. Gray, A20. <https://arxiv.org/abs/astro-ph/0405087>
- Chabrier, G., Baraffe, I., Phillips, M., & Debras, F. 2023, *A&A*, 671, A119, doi: [10.1051/0004-6361/202243832](https://doi.org/10.1051/0004-6361/202243832)
- Currie, T., Biller, B., Lagrange, A., et al. 2023a, in *Astronomical Society of the Pacific Conference Series*, Vol. 534, *Protostars and Planets VII*, ed. S. Inutsuka, Y. Aikawa, T. Muto, K. Tomida, & M. Tamura, 799, doi: [10.48550/arXiv.2205.05696](https://doi.org/10.48550/arXiv.2205.05696)
- Currie, T., Cloutier, R., Brittain, S., et al. 2015, *ApJL*, 814, L27, doi: [10.1088/2041-8205/814/2/L27](https://doi.org/10.1088/2041-8205/814/2/L27)
- Currie, T., Li, Y., El Morsy, M., et al. 2025, accepted for publication in *AJ*
- Currie, T., Burrows, A., Itoh, Y., et al. 2011, *ApJ*, 729, 128, doi: [10.1088/0004-637X/729/2/128](https://doi.org/10.1088/0004-637X/729/2/128)
- Currie, T., Debes, J., Rodigas, T. J., et al. 2012, *ApJL*, 760, L32, doi: [10.1088/2041-8205/760/2/L32](https://doi.org/10.1088/2041-8205/760/2/L32)
- Currie, T., Brandt, T. D., Uyama, T., et al. 2018, *AJ*, 156, 291, doi: [10.3847/1538-3881/aae9ea](https://doi.org/10.3847/1538-3881/aae9ea)
- Currie, T., Brandt, T. D., Kuzuhara, M., et al. 2020a, *ApJL*, 904, L25, doi: [10.3847/2041-8213/abc631](https://doi.org/10.3847/2041-8213/abc631)
- Currie, T., Guyon, O., Lozi, J., et al. 2020b, arXiv e-prints, arXiv:2012.05241. <https://arxiv.org/abs/2012.05241>
- Currie, T., Lawson, K., Schneider, G., et al. 2022, *Nature Astronomy*, 6, 751, doi: [10.1038/s41550-022-01634-x](https://doi.org/10.1038/s41550-022-01634-x)
- Currie, T., Brandt, G. M., Brandt, T. D., et al. 2023b, *Science*, 380, 198, doi: [10.1126/science.abo6192](https://doi.org/10.1126/science.abo6192)
- David, T. J., & Hillenbrand, L. A. 2015, *ApJ*, 804, 146, doi: [10.1088/0004-637X/804/2/146](https://doi.org/10.1088/0004-637X/804/2/146)
- De Rosa, R. J., Nielsen, E. L., Wahhaj, Z., et al. 2023, *A&A*, 672, A94, doi: [10.1051/0004-6361/202345877](https://doi.org/10.1051/0004-6361/202345877)
- De Rosa, R. J., Bulger, J., Patience, J., et al. 2011, *MNRAS*, 415, 854, doi: [10.1111/j.1365-2966.2011.18765.x](https://doi.org/10.1111/j.1365-2966.2011.18765.x)
- De Rosa, R. J., Patience, J., Wilson, P. A., et al. 2014, *MNRAS*, 437, 1216, doi: [10.1093/mnras/stt1932](https://doi.org/10.1093/mnras/stt1932)
- Dupuy, T. J., Liu, M. C., & Ireland, M. J. 2014, *ApJ*, 790, 133, doi: [10.1088/0004-637X/790/2/133](https://doi.org/10.1088/0004-637X/790/2/133)
- El Morsy, M., Currie, T., Kuzuhara, M., et al. 2024, in *Society of Photo-Optical Instrumentation Engineers (SPIE) Conference Series*, Vol. 13097, *Adaptive Optics Systems IX*, ed. K. J. Jackson, D. Schmidt, & E. Vernet, 130977I, doi: [10.1117/12.3019513](https://doi.org/10.1117/12.3019513)
- El Morsy, M., Currie, T., Bovie, D., et al. 2025, *ApJ*, 981, 20, doi: [10.3847/1538-4357/ada3be](https://doi.org/10.3847/1538-4357/ada3be)
- Franson, K., Bowler, B. P., Zhou, Y., et al. 2023, *ApJL*, 950, L19, doi: [10.3847/2041-8213/acd6ff](https://doi.org/10.3847/2041-8213/acd6ff)
- Franson, K., Balmer, W. O., Bowler, B. P., et al. 2024, *ApJL*, 974, L11, doi: [10.3847/2041-8213/ad736a](https://doi.org/10.3847/2041-8213/ad736a)
- Gagné, J., Faherty, J. K., Cruz, K. L., et al. 2015, *ApJS*, 219, 33, doi: [10.1088/0067-0049/219/2/33](https://doi.org/10.1088/0067-0049/219/2/33)
- Gagné, J., Mamajek, E. E., Malo, L., et al. 2018, *ApJ*, 856, 23, doi: [10.3847/1538-4357/aaae09](https://doi.org/10.3847/1538-4357/aaae09)
- Gaia Collaboration, Vallenari, A., Brown, A. G. A., et al. 2023, *A&A*, 674, A1, doi: [10.1051/0004-6361/202243940](https://doi.org/10.1051/0004-6361/202243940)
- Garcia, E. V., Currie, T., Guyon, O., et al. 2017, *ApJ*, 834, 162, doi: [10.3847/1538-4357/834/2/162](https://doi.org/10.3847/1538-4357/834/2/162)
- Greco, J. P., & Brandt, T. D. 2016, *ApJ*, 833, 134, doi: [10.3847/1538-4357/833/2/134](https://doi.org/10.3847/1538-4357/833/2/134)
- Groff, T. D., Chilcote, J., Kasdin, N. J., et al. 2016, in *Society of Photo-Optical Instrumentation Engineers (SPIE) Conference Series*, Vol. 9908, *Ground-based and Airborne Instrumentation for Astronomy VI*, 99080O, doi: [10.1117/12.2233447](https://doi.org/10.1117/12.2233447)
- Jones, J., White, R. J., Quinn, S., et al. 2016, *ApJL*, 822, L3, doi: [10.3847/2041-8205/822/1/L3](https://doi.org/10.3847/2041-8205/822/1/L3)
- Jones, J., White, R. J., Boyajian, T., et al. 2015, *ApJ*, 813, 58, doi: [10.1088/0004-637X/813/1/58](https://doi.org/10.1088/0004-637X/813/1/58)
- Jones, J. W. 2016, PhD thesis, Georgia State University
- Jovanovic, N., Guyon, O., Martinache, F., et al. 2015, *ApJL*, 813, L24, doi: [10.1088/2041-8205/813/2/L24](https://doi.org/10.1088/2041-8205/813/2/L24)
- Kervella, P., Arenou, F., & Thévenin, F. 2022, *A&A*, 657, A7, doi: [10.1051/0004-6361/202142146](https://doi.org/10.1051/0004-6361/202142146)
- Kuzuhara, M., Currie, T., Takarada, T., et al. 2022, *ApJL*, 934, L18, doi: [10.3847/2041-8213/ac772f](https://doi.org/10.3847/2041-8213/ac772f)
- Lacy, B., & Burrows, A. 2020, *ApJ*, 892, 151, doi: [10.3847/1538-4357/ab7017](https://doi.org/10.3847/1538-4357/ab7017)
- Lafrenière, D., Marois, C., Doyon, R., Nadeau, D., & Artigau, É. 2007, *ApJ*, 660, 770, doi: [10.1086/513180](https://doi.org/10.1086/513180)
- Lagrange, A. M., Bonnefoy, M., Chauvin, G., et al. 2010, *Science*, 329, 57, doi: [10.1126/science.1187187](https://doi.org/10.1126/science.1187187)

- Lozi, J., Ahn, K., Clergeon, C., et al. 2022, in Society of Photo-Optical Instrumentation Engineers (SPIE) Conference Series, Vol. 12185, Adaptive Optics Systems VIII, ed. L. Schreiber, D. Schmidt, & E. Vernet, 1218533, doi: [10.1117/12.2630634](https://doi.org/10.1117/12.2630634)
- Lucas, M., Norris, B., Guyon, O., et al. 2024, PASP, 136, 114504, doi: [10.1088/1538-3873/ad89af](https://doi.org/10.1088/1538-3873/ad89af)
- Luhman, K. L. 2023, AJ, 165, 269, doi: [10.3847/1538-3881/accf19](https://doi.org/10.3847/1538-3881/accf19)
- Luhman, K. L. 2024, AJ, 168, 159, doi: [10.3847/1538-3881/ad697d](https://doi.org/10.3847/1538-3881/ad697d)
- Luhman, K. L., Mamajek, E. E., Shukla, S. J., & Loutrel, N. P. 2017, AJ, 153, 46, doi: [10.3847/1538-3881/153/1/46](https://doi.org/10.3847/1538-3881/153/1/46)
- Marois, C., Doyon, R., Racine, R., & Nadeau, D. 2000, PASP, 112, 91, doi: [10.1086/316492](https://doi.org/10.1086/316492)
- Marois, C., Lafrenière, D., Doyon, R., Macintosh, B., & Nadeau, D. 2006, ApJ, 641, 556, doi: [10.1086/500401](https://doi.org/10.1086/500401)
- Marois, C., Macintosh, B., Barman, T., et al. 2008, Science, 322, 1348, doi: [10.1126/science.1166585](https://doi.org/10.1126/science.1166585)
- Marois, C., Zuckerman, B., Konopacky, Q. M., Macintosh, B., & Barman, T. 2010, Nature, 468, 1080, doi: [10.1038/nature09684](https://doi.org/10.1038/nature09684)
- Mawet, D., Milli, J., Wahhaj, Z., et al. 2014, ApJ, 792, 97, doi: [10.1088/0004-637X/792/2/97](https://doi.org/10.1088/0004-637X/792/2/97)
- Mesa, D., Gratton, R., Kervella, P., et al. 2023, A&A, 672, A93, doi: [10.1051/0004-6361/202345865](https://doi.org/10.1051/0004-6361/202345865)
- Minowa, Y., Hayano, Y., Oya, S., et al. 2010, in Society of Photo-Optical Instrumentation Engineers (SPIE) Conference Series, Vol. 7736, Adaptive Optics Systems II, ed. B. L. Ellerbroek, M. Hart, N. Hubin, & P. L. Wizinowich, 77363N, doi: [10.1117/12.857818](https://doi.org/10.1117/12.857818)
- Nielsen, E. L., Liu, M. C., Wahhaj, Z., et al. 2012, ApJ, 750, 53, doi: [10.1088/0004-637X/750/1/53](https://doi.org/10.1088/0004-637X/750/1/53)
- Nielsen, E. L., De Rosa, R. J., Macintosh, B., et al. 2019, AJ, 158, 13, doi: [10.3847/1538-3881/ab16e9](https://doi.org/10.3847/1538-3881/ab16e9)
- Norris, B., Schworer, G., Tuthill, P., et al. 2015, MNRAS, 447, 2894, doi: [10.1093/mnras/stu2529](https://doi.org/10.1093/mnras/stu2529)
- Pairet, B., Cantalloube, F., & Jacques, L. 2021, MNRAS, 503, 3724, doi: [10.1093/mnras/stab607](https://doi.org/10.1093/mnras/stab607)
- Pecaut, M. J., & Mamajek, E. E. 2013, ApJS, 208, 9, doi: [10.1088/0067-0049/208/1/9](https://doi.org/10.1088/0067-0049/208/1/9)
- Pueyo, L. 2016, ApJ, 824, 117, doi: [10.3847/0004-637X/824/2/117](https://doi.org/10.3847/0004-637X/824/2/117)
- Pueyo, L., Crepp, J. R., Vasisht, G., et al. 2012, ApJS, 199, 6, doi: [10.1088/0067-0049/199/1/6](https://doi.org/10.1088/0067-0049/199/1/6)
- Rose, B., Aldering, G., Hounsell, R., et al. 2023, arXiv e-prints, arXiv:2306.17226, doi: [10.48550/arXiv.2306.17226](https://doi.org/10.48550/arXiv.2306.17226)
- Royer, P., Merle, T., Dsilva, K., et al. 2024, A&A, 681, A107, doi: [10.1051/0004-6361/202346847](https://doi.org/10.1051/0004-6361/202346847)
- Service, M., Lu, J. R., Campbell, R., et al. 2016, PASP, 128, 095004, doi: [10.1088/1538-3873/128/967/095004](https://doi.org/10.1088/1538-3873/128/967/095004)
- Soummer, R., Pueyo, L., & Larkin, J. 2012, ApJL, 755, L28, doi: [10.1088/2041-8205/755/2/L28](https://doi.org/10.1088/2041-8205/755/2/L28)
- Sparks, W. B., & Ford, H. C. 2002, ApJ, 578, 543, doi: [10.1086/342401](https://doi.org/10.1086/342401)
- Stevenson, A. T., Haswell, C. A., Barnes, J. R., & Barstow, J. K. 2023, MNRAS, 526, 5155, doi: [10.1093/mnras/stad3041](https://doi.org/10.1093/mnras/stad3041)
- Tobin, T. L., Chilcote, J., Brandt, T., et al. 2020, in Society of Photo-Optical Instrumentation Engineers (SPIE) Conference Series, Vol. 11452, Software and Cyberinfrastructure for Astronomy VI, ed. J. C. Guzman & J. Ibsen, 114521D, doi: [10.1117/12.2576255](https://doi.org/10.1117/12.2576255)
- Tobin, T. L., Pal, J., Chilcote, J., et al. 2022, in Society of Photo-Optical Instrumentation Engineers (SPIE) Conference Series, Vol. 12189, Software and Cyberinfrastructure for Astronomy VII, 121892C, doi: [10.1117/12.2630368](https://doi.org/10.1117/12.2630368)
- Tobin, T. L., Currie, T., Li, Y., et al. 2024, AJ, 167, 205, doi: [10.3847/1538-3881/ad3077](https://doi.org/10.3847/1538-3881/ad3077)
- Wenger, M., Ochsenbein, F., Egret, D., et al. 2000a, A&AS, 143, 9, doi: [10.1051/aas:2000332](https://doi.org/10.1051/aas:2000332)
- Wenger, M., Ochsenbein, F., Egret, D., et al. 2000b, A&AS, 143, 9, doi: [10.1051/aas:2000332](https://doi.org/10.1051/aas:2000332)
- Winterhalder, T. O., Kammerer, J., Lacour, S., et al. 2025, A&A, 700, A4, doi: [10.1051/0004-6361/202554766](https://doi.org/10.1051/0004-6361/202554766)
- Wolff, S. G., Wang, J., Stapelfeldt, K., et al. 2024, in Society of Photo-Optical Instrumentation Engineers (SPIE) Conference Series, Vol. 13092, Space Telescopes and Instrumentation 2024: Optical, Infrared, and Millimeter Wave, ed. L. E. Coyle, S. Matsuura, & M. D. Perrin, 1309255, doi: [10.1117/12.3020205](https://doi.org/10.1117/12.3020205)
- Zhang, Y., Xuan, J. W., Mawet, D., et al. 2024, AJ, 168, 131, doi: [10.3847/1538-3881/ad6609](https://doi.org/10.3847/1538-3881/ad6609)